LARGE-AREA AMORPHOUS SILICON TFT-BASED X-RAY IMAGE SENSORS FOR MEDICAL IMAGING AND NON DESTRUCTIVE TESTING

Richard L. Weisfield

dpiX, LLC
3406 Hillview Ave.
Palo Alto, CA 94034-1345

Large-format digital x-ray image sensors are a recent development in the fields of medical imaging and non-destructive testing. Such image sensors have become practical through the emergence of large-area, amorphous Silicon (a-Si) TFT and photodiode technologies (1,2). This paper will review the fundamental requirements for such x-ray image sensors, and discuss some of the device requirements for TFTs and photodiodes which serve as the basic components in each pixel.

INTRODUCTION

X-ray imaging has been used in a variety of contexts, including high resolution imaging using film, real-time video imaging using image intensifier tubes, and digital imaging for digital subtraction angiography and computer-aided tomography. Additional uses of digital x-ray imaging include bone mineral densitometry, portal imaging for radiotherapy, and many areas of materials monitoring which use x-rays for nondestructive testing. In many of these applications, a large-area flat-panel imager based on a-Si thin-film transistor (TFT) technology is an attractive component due to its light weight and small form-factor, high photosensitivity, and lack of image distortion that is present in image intensifier tubes.

These different applications place unique requirements on the image sensor. In the case of x-ray film replacement, the most important characteristics are high resolution and dynamic range, as well as large-area image format. In the case of real-time video imaging for fluoroscopy and other digital medical imaging applications, low noise and high detective quantum efficiency are especially important, since such images are often taken under very low levels of x-ray illumination. For non-destructive testing applications, low dose is not so critical, but high dynamic range and rapid image capture are typically emphasized.

TFT / Photodiode Array

Many of these applications can be met using a large-area array of a-Si TFTs and photodiodes. The TFTs are used as pixel switches which address each row of the array,

and photodiodes at each pixel location convert incident light to charge, which is read out by charge amplifiers connected to each column of the array. The arrangement of such elements is shown in Figure 1. Each row contains a gate line which connects to the gate of each TFT. Each column contains a data line which connects to the source of each TFT and a bias line which connect to each photodiode. The arrays operate in charge integration mode, that is, the photodiodes integrate photocurrent over a frame time (typically msecs. to secs.), and the charge is read out when each gate line is turned on (typically 10 –20 μsec.)

The pixel structure is shown in cross-sectional form in Figure 2. In this cross-section one can see the TFT and photodiode embedded within a pixel. A photomicrograph of a 127 μm pixel is shown in Figure 3. It is clear that the TFT and metal addressing lines take up a significant fraction of the pixel, so that the photosensitive fraction of the pixel, defined as the pixel fill-factor, is 57% in this embedded photodiode architecture.

X-ray Scintillators

X-ray phosphors are generally optimized to emit most efficiently in the visible spectrum, which is well matched to the spectral response of a-Si photodiodes. In order to detect x-rays, an x-ray conversion screen is placed over the array whose purpose is to absorb x-rays and scintillate in the visible spectrum. $Gd_2O_2S(Tb)$, a common material used in x-ray film cassettes, serves as an efficient screen material, and can be obtained in various coating thicknesses and densities to optimize resolution and sensitivity. An alternative approach is to coat the array with CsI(Tl) which has a columnar structure that provides a kind of light-piping effect, allowing thicker, more absorptive films to be used with less light spreading than in conventional phosphor screens

ARRAY PERFORMANCE

a-Si Photodiode

The photodiode used in these applications is an a-Si photodiode made in the *nip* structure. Such photodiodes can have quantum efficiencies greater than 80% in the wavelength region of 500 to 600 nm. The quantum efficiency is tailored as in a-Si solar cells by using thin, wide bandgap *p*-layers, and optimizing the overlying passivation and contact layers to maximize light transmission from the phosphor into the photodiode. A typical quantum efficiency reponse curve *vs.* wavelength is shown for an *nip* photodiode in Figure 4. These measurements, taken at -5 V reverse bias, indicate that the average quantum efficiency in the green part of the spectrum where typical phosphors luminesce

is greater than 70%. Undulations in spectral response *vs*. wavelength due to thin film interference effects are not apparent, but these variations are considerably reduced when the phosphor layer is index-matched to the photodiode passivation layer.

Other requirements of the photodiode are low dark current, low capacitance for improved speed and lower noise, and fast photoresponse, which are characteristics not normally required of a-Si solar cells. Using an *nip* structure, one can achieve these properties, including room temperature dark currents of less than 1 pA / mm^2 with -5 Volts reverse bias. These low leakage currents allow imagers to operate without cooling and integrate for frame times of greater than 30 seconds, useful for low light level applications. A plot of dark and photocurrent vs. reverse bias is shown in Figure 5. The photocurrent is very flat with reverse bias, which provides good linearity of response, until the voltage across the photodiode drops to zero under saturation conditions.

a-Si TFT

The other important element of the array is the TFT. The TFT allows the photodiodes to integrate charge over long periods of time and sequentially transfer their stored charge to individual datalines simultaneously. The TFT is required to have low enough off-current (typically a few fA) to suppress crosstalk among all the pixels connected to each dataline. In addition, the TFT must have sufficiently low on-resistance (typically a few MOhms) to transfer the stored pixel charge to the dataline in a few microseconds in order to achieve high frame rates. These requirements are well matched to the performance of a-Si TFTs, as shown in a typical TFT transfer curve shown in Figure 6.

An example of how the TFT is used to transfer charge from the photodiode to a charge amplifier is shown in Figure 7. In this example, we compare two experimental cases, one in which a 150 μm x 150 μm photodiode is in the dark, the other where the photodiode is under constant illumination. The bias is kept at –5 V and the gate is switched from –8 V to + 15 V. The data is read out with a charge amplifier. Also shown are SPICE model simulations for these two cases. The two important features in the transfer process is the presence of feedthrough charge produced whenever the TFT turns on or off, and the transient behavior of the charge transfer process which occurs when the photodiode is illuminated. In sensor imaging applications a double correlated sampling technique is used in which the dataline is sampled immediately prior and directly after the gates are turned on and off. This approach reduces low frequency noise.

The SPICE model evidently underestimates the amount of feedthrough observed experimentally, probably not taking into full account the parasitic sources of gate to drain and gate to source coupling within the pixel. The model does properly account for the

time required for the TFT to discharge the pixel, which is important for achieving adequate charge transfer efficiencies (typically greater than 95%).

Array Readout Noise

One of the most important considerations in imager performance is electronic noise. The main source of noise in large-area arrays arises from dataline capacitance, which is typically 50 to 100 pF, depending on the size of the array. The dataline capacitance serves as a parasitic element which multiplies any voltage noise on the dataline into a large charge noise on the output of each charge amplifier. A fundamental goal of array design, therefore, is to minimize dataline capacitance. This is done through a combination of TFT geometry, line width, crossover size, and dielectrics used. Future improvements in array performance will benefit from fully self-aligned TFTs and low k dielectric material to further minimize dataline capacitance.

Another element in reducing electronic noise is accomplished through charge amplifier design and readout method. Most image sensors utilize very high gain, high dynamic range charge amplifiers, which incorporate a feedback capacitor of comparable size to that of the photodiode capacitance. In addition, readout schemes such as double-correlated sampling are employed to electronic noise.

A summary of the way readout noise scales with array size is shown in Figure 8. The base component is pixel-level noise, which scales with pixel size, but is independent of array size. It is usually a relatively small component of overall noise. The more dominant source of noise is that arising from the parasitic noise associated with the charge amplifier connected to a high capacitance data line. In addition, thermal noise associated with resistance in the data lines becomes quite significant in the largest arrays. Efforts to minimize data line resistance and capacitance are important goals of future designs.

X-Ray Detector System

An x-ray imaging detector with 127 micron pixels and 30 x 40 cm^2 active area has recently been developed (2). The array has over 7 million pixels. A photograph of the array bonded to gate and data boards is shown in Figure 9. The array is bonded using TAB packaging utilizing technology identical to that used in making flat panel displays. The entire system consists of the array module, a $Gd_2O_2S(Tb)$ or other phosphor screen, and ADC, logic, and power regulator boards, which connect to an external power supply and PC frame grabber card. The system can take 12 bit images every 3 seconds, and produces images with excellent fidelity and dynamic range.

Imaging Examples

Some examples of images taken with this detector are shown in Figures 10 to 12. They show the image of a hand phantom, a chest image, and a bullet passing through a light bulb, captured under x-ray strobe illumination. Clearly, many exciting applications for digital x-ray images, both in the medical diagnostic and nondestructive imaging fields, are envisioned.

FUTURE OPPORTUNITIES

In the future, the requirement for higher resolution will be important. As pixel size decreases, the need to increase sensitivity will become more important. One way to improve sensitivity is to increase sensor fill-factor. A new pixel architecture, where the photodiode is stacked on top of the TFT matrix, is one approach to accomplish this goal. A cross-section of a high fill-factor architecture is shown in Figure 13. In this approach, the bottom *n*-type contact to the photodiode is segmented, but the rest of the *i* and *p* layers are continuous. The dependence of fill factor and dynamic range with pixel size for the embedded and stacked photodiode architectures are shown in Figures 14 and 15, respectively. It is clear that using a high fill-factor approach can provide great benefits in dynamic range for pixel sizes smaller than 100 μm. Work is presently in progress evaluating the viability of such approaches.

REFERENCES

1. R.L. Weisfield, R.A. Street, R.B. Apte, A. Moore, **SPIE 3032**, p. 14, Physics of Medical Imaging (1997).

2. R.L. Weisfield, M.A. Hartney, R.A. Street, R.B. Apte, **SPIE 3336**, p. 444, Physics of Medical Imaging (1998).

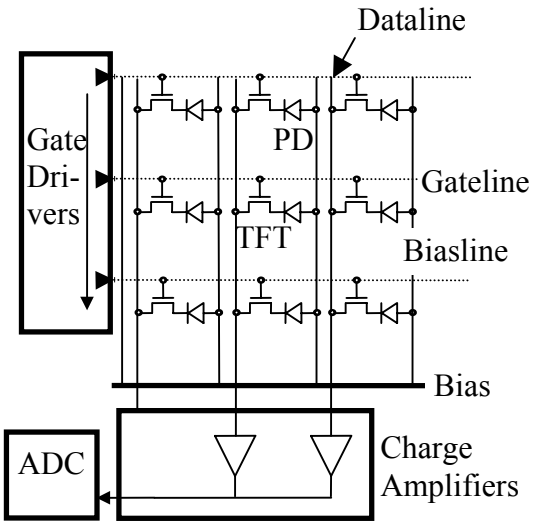

Figure 1: Diagram of TFT/Photodiode array configuration, connected to gate drivers, charge amplifiers, and analog-to-digital converters.

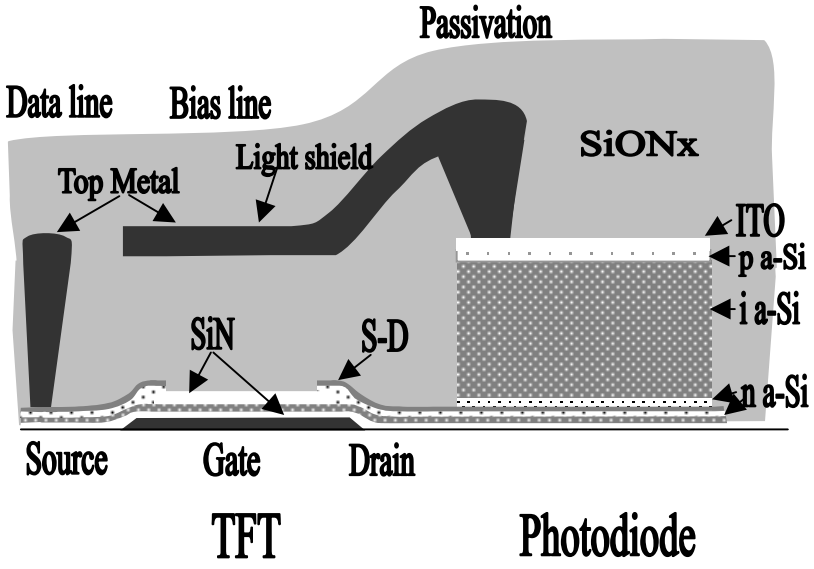

Figure 2: Cross-sectional diagram of a standard pixel in which the photodiode is embedded within the same plane as the TFT and addressing lines.

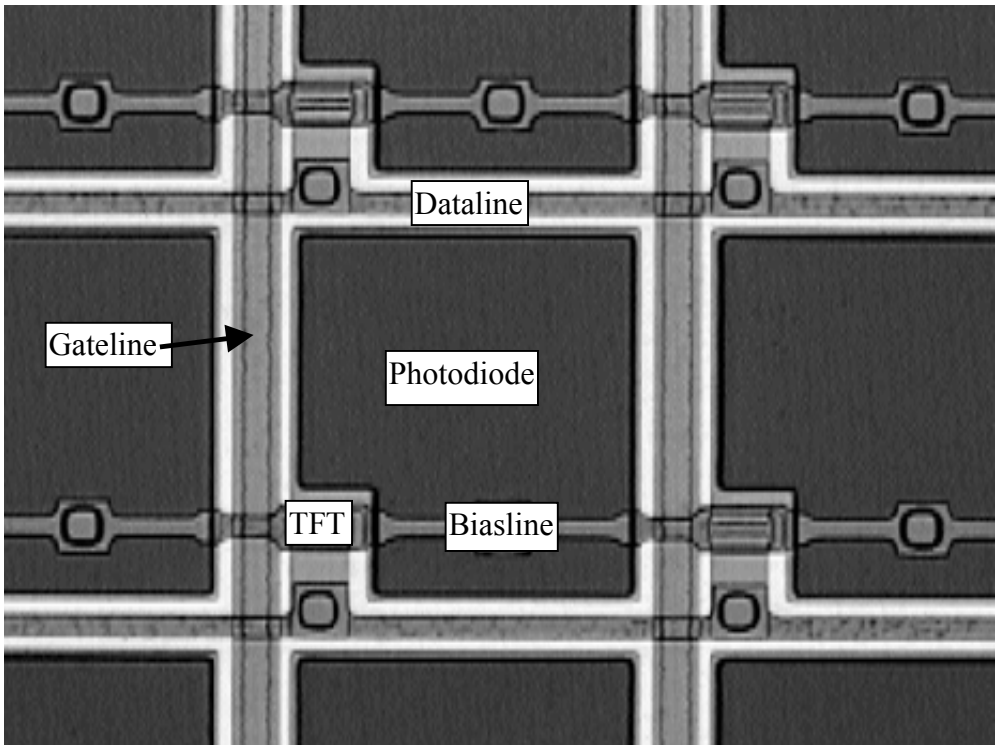

Figure 3: Photomicrograph of a 127 μm pixel.

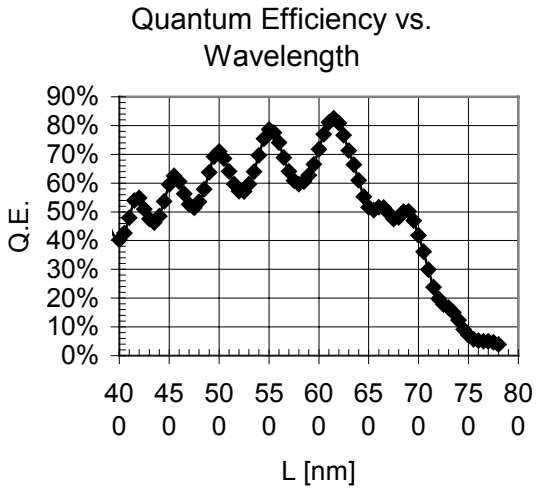

Figure 4. Spectral response of a typical a-Si *nip* photodiode at –5 V reverse bias vs. wavelength.

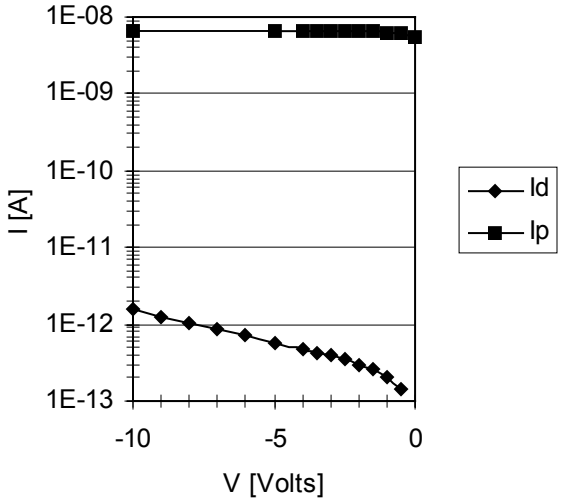

Figure 5: I(V) curve of a 1 mm^2 *nip* photodiode in the dark (Id) and under 570 nm illumination (Ip).

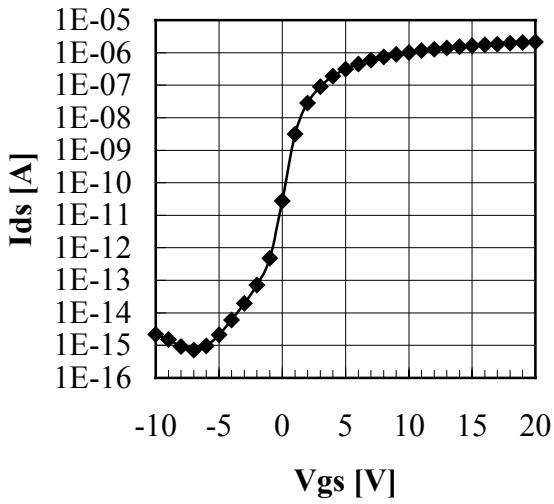

Figure 6: Typical I(Vgs) characteristic of an a-Si TFT at Vds = 5 V, with width W = 20μm and length L= 10 μm (measured on 500 TFTs in parallel).

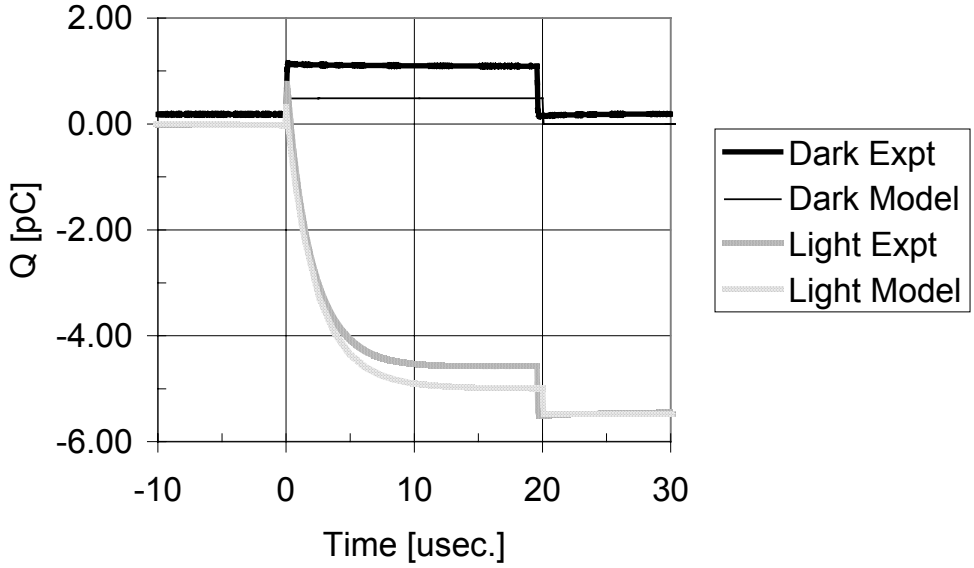

Figure 7: Charge transfer process when gate voltage is changed from –8 to +15 V from t=0 to t=20 μsec. Two cases are shown, one in the dark and one under illumination. Experimental data are compared against Spice modeling for a 150 μm pixel.

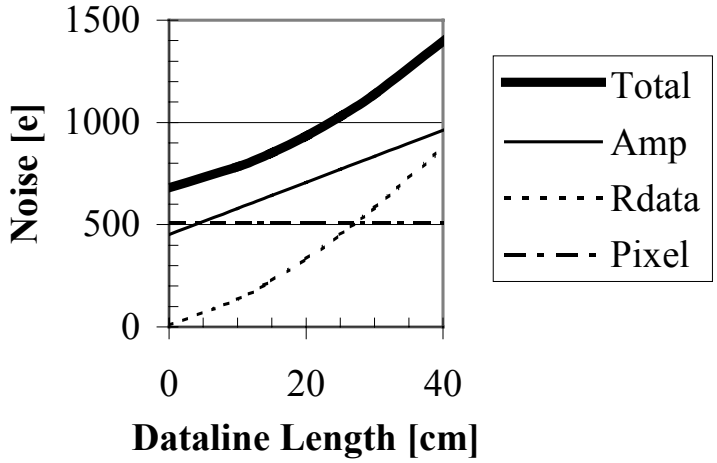

Figure 8: Various contributions of electronic noise associated with pixel size and dataline length. The dashed line is the pixel level noise; the dotted line is the thermal noise generated by the dataline resistance; the fine line is the noise generated by a high quality charge amplifier; and the bold line is the total noise taking these three contributions in quadrature.

Figure 9: A 30 x 40 cm active area 127 μm pixel image sensor module with gate and data boards TAB bonded to the glass, which is mounted on an aluminum backing plate.

Figure 10: A digital x-ray image of a human hand phantom.

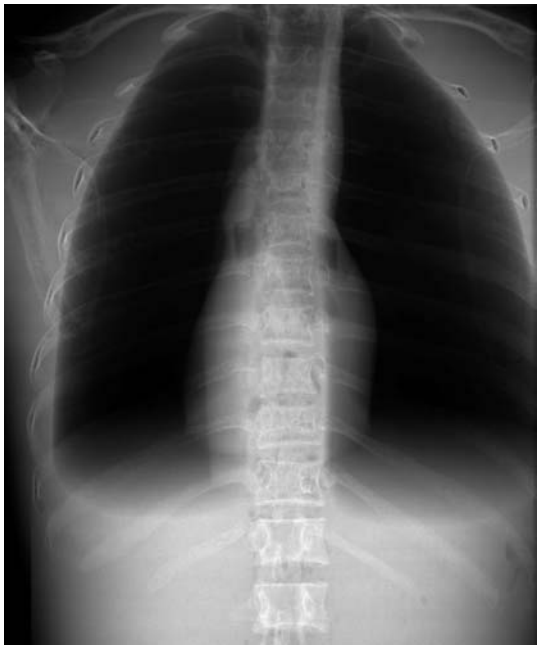

Figure 11. A digital x-ray image of a human chest phantom.

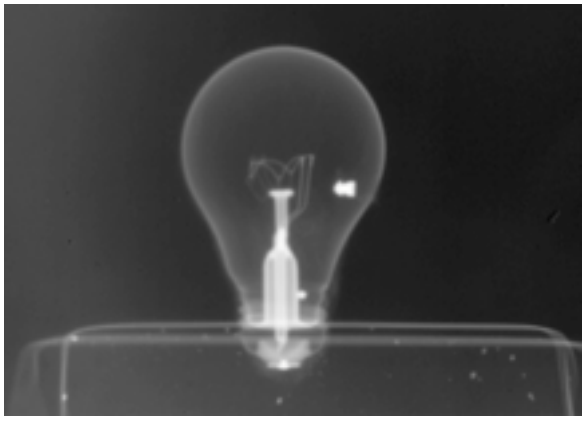

Figure 12: A digital x-ray of a bullet fired into a light bulb, taken with a fast x-ray pulse.

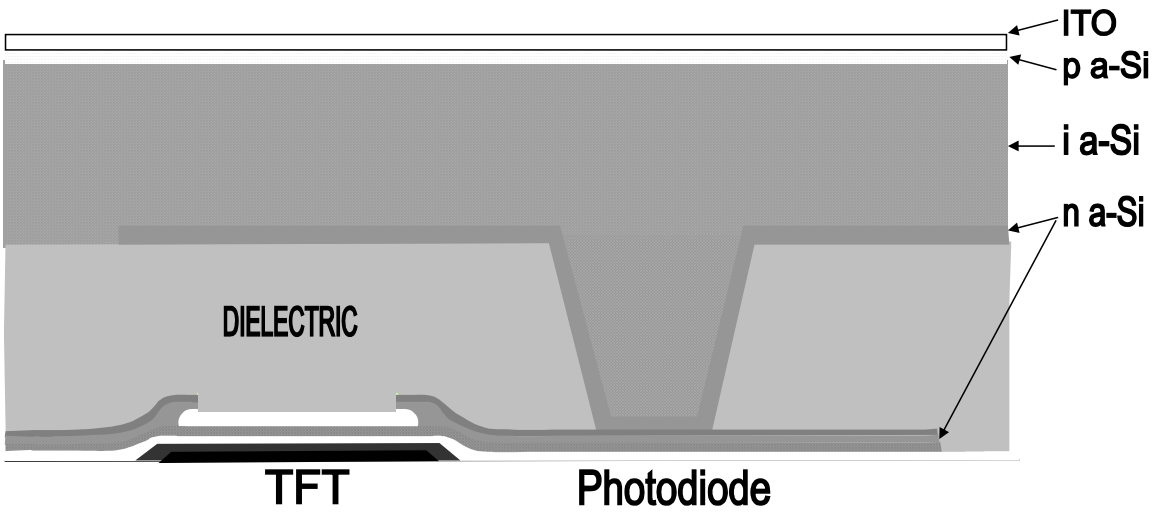

Figure 13: A high fill-factor sensor architecture in which the photodiode is stacked on top of the TFT and addressing lines.

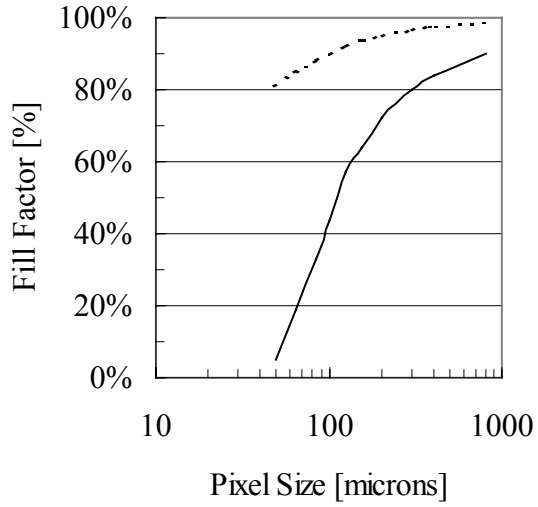

Figure 14: Sensor fill factor *vs.* pixel size for embedded (solid line) and stacked (dotted line) photodiode architectures.

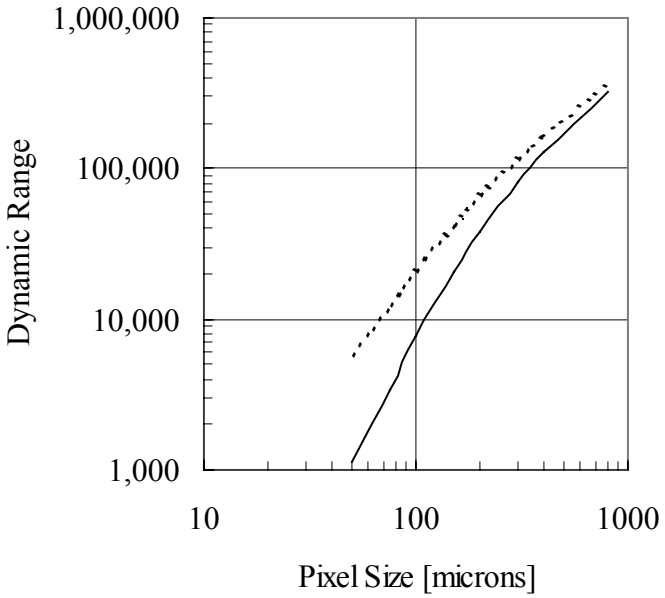

Figure 15: Sensor dynamic range (maximum signal divided by projected electronic noise) *vs*. pixel size for embedded (solid line) and stacked (dotted line) photodiode architectures.

Key Words

a-Si, TFT, photodiode, x-Ray, detector, imager, sensor, fill-factor